# Methionine γ-lyase Traps Cofactor Pyridoxal-5′-phosphate through Specific Serine-Mediated Affinity

Chang Yan[1†], Xueting Liu[1†], Ruiqi Su[1], Mengwen Shi[2], Zhi Geng[1], Ying Chen[1], Liwen Zhu[1], Zongjie Dai[3], Junfeng Hui[4], Xi Chen[2]* & Kai-Zhi Jia[1]*

[1]Cooperative Innovation Center of Industrial Fermentation (Ministry of Education & Hubei Province), Key Laboratory of Fermentation Engineering (Ministry of Education), Hubei Key Laboratory of Industrial Microbiology, National "111" Center for Cellular Regulation and Molecular Pharmaceutics, Hubei University of Technology, Wuhan 430068, China.

[2] Key Laboratory of Synthetic and Natural Functional Molecule of the Ministry of Education, College of Chemistry and Materials Science, Northwest University, Xi'an, 710127, China.

[3]Tianjin Institute of Industrial Biotechnology, Chinese Academy of Sciences, Tianjin 300308, China.

[4]Shaanxi Key Laboratory of Biomaterials and Synthetic Biology, Shaanxi R&D Center of Biomaterials and Fermentation Engineering, School of Chemical Engineering, Northwest University, Xi'an, 710127, China

[†]These authors contributed equally to this work.

Classification: Biochemistry

Keywords: methionine γ-lyase | cofactor | affinity

*Corresponding author: Xi Chen, tel & fax: +86-13709211908, e-mail: xchen@nwu.edu.cn;

Kai-Zhi Jia, tel & fax: +86-027-59750483, e-mail: kaizhijia1@163.com, kaizhijia@hbut.edu.cn

## ABSTRACT

Pyridoxal-5′-phosphate (PLP), the ubiquitous and ancient cofactor, plays important roles in enzymatic elimination, transamination and other reactions. The catalytic efficiency of PLP-dependent enzymes is significantly higher than that of free PLP. The recruitment of PLP from the environment by the enzymes, particularly through interactions outside the active site, is the key step determining the occurrence of PLP-mediated catalysis. However, the precise mechanism by which enzymes recruit PLP remains elusive. Methionine γ-lyase (MGL), a PLP-dependent enzyme, catalyzes the degradation of L-methionine, thereby suppressing cancer cell proliferation through serum or dietary methionine depletion. Here, we report the crystal structure of yMGL, which belongs to a newly identified subgroup of cystathionine γ-lyases, in complex with L-methionine and PLP. Through truncating the C-terminal domain of yMGL both *in vitro* and *in vivo*, we demonstrated that this domain, outside the canonical PLP-binding domain, is essential for the specific interaction between yMGL and PLP, as well as for efficient L-methionine catabolism. The C-terminal domain, which contains a conserved serine residue, forms a unique structural feature at the enzyme's entrance that effectively traps PLP and confers PLP specificity. These findings elucidate a previously uncharacterized mechanism of PLP recruitment by MGLs and offer a structural framework to rationally design and engineer MGLs with tailored cofactor selectivity and catalytic performance.

## SIGNIFICANCE

Understanding the mechanism by which enzymes recruit cofactors is essential for advancing biochemistry and developing biotechnological applications. PLP is a ubiquitous and ancient cofactor required by numerous metabolic enzymes. Despite its fundamental importance, the molecular mechanisms governing how enzymes selectively recruit and bind PLP from the environment remain poorly understood. Our structural and functional analysis of methionine γ-lyases and their ancestral enzymes reveals a previously unknown PLP recruitment mechanism involving a C-terminal domain that acts as a cofactor trap outside the canonical active site. This discovery advances our understanding of enzyme-cofactor interactions and provides a rational framework for designing and engineering PLP-dependent enzymes.

## INTRODUCTION

Pyridoxal-5′-phosphate (PLP), the biologically active form of vitamin B6, serves as a ubiquitous and highly versatile cofactor in enzymatic catalysis, particularly in the metabolism of amino acids; the biosynthesis of antibiotics such as indolmycin and azomycin; and the production of key neurotransmitters, including serotonin, dopamine, epinephrine, norepinephrine, gamma-aminobutyric acid (GABA), and histamine.(1-3) PLP-dependent enzymes catalyze elimination, transamination, decarboxylation, racemization, substitution, and retro-aldol cleavage reactions and are estimated to account for ~ 4% of all enzyme activities.(4) Despite extensive studies, the functional repertoire of PLP-dependent enzymes continues to expand, with newly discovered reactions and previously unannotated proteins being reported in recent years.(5) The remarkable catalytic versatility of PLP arises from its unique chemical features. By acting as an “electron sink”, PLP delocalizes electron density through its conjugated pyridine ring via resonance, thereby stabilizing high-energy intermediates during catalysis.(6) Central to its function is the formation of a Schiff base (internal aldimine) with a conserved lysine at the active site, which is subsequently displaced by the substrate to form an extermal aldimine.(7) This transformation enables a variety of key reactions, including decarboxylation, deprotonation and carbanion stabilization through the quinonoid intermediate, to proceed under physiologically mild conditions.(8) PLP-mediated enzymatic catalysis follows the recruitment of PLP from the environment, especially through interactions outside the active site. However, the precise mechanism by which enzymes recruit PLP remains unclear.

Amino acids, as prototypical substrates of PLP-dependent enzymes, likely play crucial roles in prebiotic chemistry.(9) In the context of early Earth, amino acids might have been synthesized, transformed and degraded through nonenzymatic reactions under plausible primordial conditions.(10-12) These transformations might have been mediated by PLP-like molecules, which are

thermodynamically favorable and readily formed.(9, 13) During molecular evolution, PLP is thought to have initially associated with RNA (RNA-PLP) and later evolved to function within protein scaffolds, enabling greater diversity and efficiency of chemical reactions.(9) The recruitment of PLP by enzymes would have conferred a significant selective advantage by accelerating amino acid turnover, an essential process for cellular growth and adaptation. Notably, enzymatic PLP catalysis proceeds $10^7$ to $10^9$ times faster than PLP catalysis alone,(12, 14) underscoring the importance of PLP capture as a rate-limiting and evolutionarily critical step in metabolism. Understanding how enzymes capture PLP is therefore essential for elucidating cofactor-driven molecular evolution and guiding enzyme engineering strategies.

Methionine γ-lyase (MGL), a representative PLP-dependent enzyme, catalyzes the γ-elimination of L-methionine (L-Met), yielding α-ketobutyric acid, methanethiol and ammonia. MGLs are members of the cystathionine γ-lyase family and contribute to the production of volatile organosulfur compounds, with implications for cardiovascular health, evolution of life and flavor biosynthesis.(15, 16) MGLs exhibit therapeutic significance by depleting L-Met in biological systems, thereby inhibiting cancer progression and promoting healthspan and longevity.(17-19) Although PLP is required throughout the methionine cleavage reaction, the mechanism by which MGLs recruit PLP prior to catalysis remains unknown.(7)

In this study, we investigated the mechanism of PLP recruitment by MGL from *Yarrowia lipolytica* (yMGL, KEGG ID: YALI0C22088g), a strain noted for its robust L-Met degradation capacity.(16) We solved the crystal structure of yMGL in complex with the substrate L-Met and cofactor PLP, elucidated the molecular interactions between PLP and yMGL *in vitro*, and demonstrated the *in vivo* relevance of this interaction for L-Met catabolism. Through a combination of biochemical and genetic characterization, supported by structural modeling, we identified the C-

terminal region as a key determinant of PLP binding specificity. Furthermore, site-directed mutagenesis, PLP binding affinity assays together with conservation analysis revealed a conserved residue critical for PLP recognition across MGLs. These findings provide mechanistic insights into cofactor recruitment and highlight the evolutionary adaptation of PLP-dependent enzymes to enhance specificity and catalytic efficiency. Our work not only deepens the understanding of PLP-enzyme interactions but also lays a foundation for rational engineering of cofactor-dependent enzymes.

## RESULTS

### The structure of the yMGL-L-Met-PLP complex

yMGL belongs to a newly identified subgroup of cystathionine γ-lyases in yeast and is phylogenetically distinct from the other structurally characterized or functionally annotated cystathionine γ-lyases (Fig. 1*A*).(16) The X-ray crystal structure of yMGL in complex with the cofactor PLP and substrate L-Met was determined (PDB ID: 9UUW). The enzyme adopts a dimeric architecture, with the active site formed at the interface between adjacent monomers (Fig. 1*B*-*F*). Each monomer consists of three domains: an N-terminal domain (residues 7-63), a PLP-binding domain (residues 64-261) and a C-terminal domain (residues 262-380) (Fig. 1*B*). At the active site of chain A, PLP is covalently linked to the ε-amino group of K204, forming a Schiff base. The phosphate group of PLP forms hydrogen bonds with G91 and T203. The carboxylate group of L-Met forms salt bridges with R344 and R357, and its amino group forms a hydrogen bond with T332 (Fig. 1*C* and *D*). At the active site of chain B, PLP is similarly linked to K204 via a Schiff base. However, L-Met is positioned farther from the aldimine linkage (Fig. 1*E* and 1*F*). The PLP phosphate interacts via hydrogen bonds with Y61 (A chain), L92 and T203 and forms a salt bridge with R63 (A chain). A π–π stacking interaction is observed between the PLP aromatic ring and Y113. L-Met is stabilized

through salt bridges with R334 and R357 (Fig. 1*E*).

The dimeric structure of yMGL closely resembles those of hMGL and pMGL, with Cα r.m.s.d. values of 1.17 Å and 1.18 Å, respectively (Fig. 1*H* and *SI Appendix*, Fig. S1*A*). Notably, yMGL contains an extended loop adjacent to the active-site lid, whereas the corresponding regions in the thermophilic enzymes hMGL and pMGL comprise several α-helical elements (*SI Appendix*, Fig. S1*A*). yMGL exhibits cold tolerance (*SI Appendix*, Fig. S1*B*,*C*), and this extended loop may represent a structural adaptation that facilitates function at low temperatures. (20)

The predicted entrance and active site of yMGL consists of a total of 33 amino acid residues (Fig. 2). Through alanine (Ala) scanning mutagenesis combined with L-Met degradation assays, we identified 22 key amino acid residues, which are highlighted in the primary structure of yMGL (Fig. 2*E*). Notably, the majority of these essential residues, spanning from A28 to S244, are located within the N-terminal domain and PLP-binding domain (Fig. 2*A*, *C* and *D*), with only one, S333, residing in the C-terminal domain (Fig. 2*A*, *D* and *E*). These observations led us to further investigate the functional role of the C-terminal domain.

**Truncation of the C-terminal domain of yMGL**

To investigate the functional role of the C-terminal domain in yMGL, we generated a truncated variant, yMGL-ΔCTD, by deleting residues 253-380 (Figs. 2*E* and 3*A*). The theoretical molecular weights of yMGL and yMGL-ΔCTD as monomers are 41.93 kDa and 27.77 kDa, respectively, which is consistent with the results of the SDS–PAGE analysis (Fig. 3*B*,*C*). Size exclusion chromatography revealed that both proteins eluted as single peaks, corresponding to apparent native molecular weights of ~150 kDa for yMGL and 157 kDa for yMGL-ΔCTD (Fig. 3*D* and *SI Appendix*, Fig. S2*A*). Dynamic light scattering analysis further revealed that yMGL-ΔCTD exhibited a larger hydrodynamic radius

than yMGL did (Fig. 3*E*), suggesting that C-terminal truncation altered the quaternary structure from a homotetramer to a homohexamers at pH 8.0. This structural shift was accompanied by an alteration in the CD spectra (*SI Appendix*, Fig. S2*B*). More importantly, compared with full-length yMGL, yMGL-ΔCTD exhibited a 7.20-fold increase in L-Met degradation activity at optimal enzymatic reaction temperature (Fig. 3*F*). However, the activity of yMGL-ΔCTD decreased more sharply at lower temperatures (*SI Appendix*, Fig. S2*C,D*), indicating reduced kinetic and thermodynamic stability (Table 1 and *SI Appendix*, Figs. S2*D-F* and S3). The kinetic parameters of yMGL and yMGL-ΔCTD were determined using L-Met as the substrate under saturating PLP concentrations (Table 1 and *SI Appendix*, Fig. S3*A,C*). The catalytic efficiency of the yMGL-ΔCTD was 33.33% higher than that of the wild-type enzyme, which is closely associated with an enhanced binding ability for the L-Met (Table 1 and *SI Appendix*, Fig. S3*A,C*). However, when the L-Met concentration was maintained at saturation and the PLP concentration was varied, the catalytic efficiency of yMGL-ΔCTD decreased by 10.65-fold relative to that of yMGL (Table 1 and *SI Appendix*, Fig. S3*B,D*). These findings suggest that the C-terminal domain may contribute to the specificity of yMGL for PLP.

**Functional analysis of the C-terminal domain of yMGL**

Binding affinity, a key indicator of substrate specificity in enzymes,(21-23) was used to assess changes in specificity toward PLP among yMGL, yMGL-ΔCTD and the isolated C-terminal domain (yMGL-CTD). As shown in Table 1, the equilibrium dissociation constant (KD), reflecting the PLP-binding affinity, was $3.31 \times 10^{-5}$ M for yMGL (Fig. 4*A*). In contrast, no detectable binding signal was observed for yMGL-ΔCTD (Fig. 4*B*), whereas the KD value for yMGL-CTD was $1.03 \times 10^{-5}$ M, closely resembling that of the full-length yMGL (Fig. 4*C*). These data indicate that the C-terminal domain of yMGLs determines their specific affinity for PLP.

The presence or absence of PLP had no significant effect on the CD spectra of either yMGL or yMGL-ΔCTD (*SI Appendix*, Fig. S2*B*). To assess whether the C-terminal domain implicated in PLP specificity is essential for degrading L-Met *in vivo*, we deleted the whole gene encoding yMGL or the sequence encoding the C-terminal domain by using a CRISPR–Cas9 system integrated with homologous recombination technology. The deletion genotypes were confirmed by observing the reduction in the PCR product size and sequencing the PCR products (*SI Appendix*, Fig. S4). Analysis of growth profiles and metabolite accumulation revealed that deletion of either *yMGL* or its C-terminal domain significantly increased cell density (Fig. 4*D*) and abolished both the intracellular and the extracellular accumulation of keto acids, particularly during the late stages of fermentation (Fig. 4*E*,*F*). Supplementation with L-Met exacerbated the accumulation of keto acids in the wild-type strain but had no effect on either mutant (Fig. 4*E*,*F*). Transcriptomic and metabolomic analyses further indicated that truncation of the C-terminal domain led to transcriptional downregulation of *yMGL*, accompanied by a reduced accumulation of α-ketobutyric acid, compared with that in the wild-type strain (Fig. 4*G*-*I*). Additionally, we observed the formation of an extracellular pool of α-ketobutyric acid in the wild-type strain in response to L-Met addition, likely due to active excretion driven by its cytotoxic potential (Fig. 4*H*-*I*).(24) The similarity in phenotype between the two mutants in terms of growth and L-Met degradation supports the conclusion that the C-terminal domain, through its specific interaction with PLP, plays a critical role in regulating enzymatic L-Met degradation.

**Key amino acid residues in the C-terminal region that determine the specific action of PLP**

The homotetramer structure of yMGL within the enzymatic system was modeled by assembling two dimeric units (Fig. 5*A*). The C-terminal domains extend across the active site and are positioned above its entrance (Fig. 5*A*-*C*). Upon docking of PLP with the C-terminal domain of yMGL, residues R255,

K270 and S333 were predicted to interact with PLP (Fig. 5*A*). The alanine substitution of these three residues in yMGL-CTD abolished expression in *E. coli* (data not shown). Consequently, site-directed mutagenesis was performed in the full-length yMGL. Among the three single-point mutants, only S333A resulted in a complete loss of L-Met degradation activity, accompanied by a 27.54-fold reduction in the binding affinity of PLP (Fig. 5*D*). Furthermore, the S333A mutant exhibited a 3.4 °C decrease in melting temperature (an indicator reflecting the substrate specificity), suggesting that S333 determines the specific interaction between the C-terminal domain and PLP (Fig. 5*E*,*F* and *SI Appendix*, Fig. S5). However, S333 anchores near the entrance and does not appear to engage in direct interactions with PLP at the active site (Fig. 5*A*-*C*). It resides within a loop region, and dynamic analysis revealed that the S333A mutation did not trigger significant structural fluctuations across the entire yMGL protein, leading us to hypothesize that yMGL may utilize a PLP-trapping mechanism centered on S333 at the vicinity of the entrance (Fig. 5*A* and *G*-*H*). Notably, this Ser residue is highly conserved among MGL homologs (Fig. 2*E*). The corresponding mutation of S340 to alanine in human MGL into Ala, located at the entrance of the active site (Fig. 6*A*), significantly reduced both PLP affinity and specificity, the S340A mutant exhibited a 7.6 °C decrease in melting temperature (Fig. 6*B*,*C*), further substantiating our hypothesis.

To investigate the evolutionary adaptation of MGLs to recruit PLP, we utilized an ancestral sequence reconstruction strategy to obtain putative ancestral enzymes. Ten different ancestral nodes were inferred from the phylogenetic tree of the yMGL subfamily (Fig. 7*A*). Sequence analysis revealed that the Ser residue is conserved in both yMGL and its ancestral variants (Fig. 7*A*). Interestingly, many cystathionine γ-synthases were included in the phylogenetic tree, as provided by the FireProt database, to assist in identifying the evolutionary origins of yMGL (Fig. 7*A*). This observation led us to hypothesize that yMGL may exhibit cystathionine γ-synthase activity. This

hypothesis was supported by detecting the production of succinic acid in the enzymatic reactions using L-cysteine and O-succinyl-L-homoserine as the substrates (Fig. 7*B*). Loopy proteins appear to be evolutionarily conserved.(25) Compared with pMGL and hMGL, yMGL features longer loops (*SI Appendix*, Fig. S1*A*), which contribute to its enhanced substrate promiscuity, which is consistent with its bifunctional activity as both a cystathionine γ-synthase and a cystathionine γ-lyase, including methionine γ-lyase activity. All of these PLP-dependent enzymes possess a conserved Ser residue located within a putative PLP-trapping structure near the entrance of active site (Fig. 7*C*-*E*). Based on these findings, we propose that these enzymes may have evolved a common mechanism to recruit PLP through this trap structure, wherein the conserved Ser residue facilitates specific interaction with the cofactor PLP.

## DISCUSSION

yMGL represents a newly identified subgroup within the cystathionine γ-lyase family. In this study, its structure was solved (PDB ID: 9UUW) and the C-terminal domain of yMGL, outside the canonical PLP-binding domain, determines the specific PLP affinity and L-Met degradation (Figs. 1 and 4*A*-*C*). Ser within this domain was found to interact specifically with PLP (Fig. 5*D*-*F*), a feature preserved in yMGL, its ancestors and the other MGLs (Fig. 7*A* and *C*-*E*).

Loop regions originating from the C-terminal domain were found to reside near the active site entrance of MGLs (Fig. 5*A*-*C*), potentially acting as a PLP-trapping module that facilitates PLP entry and guides it into the hydrophobic pocket to increase its catalytic efficiency. Truncation of the C-terminal domain altered the overall structural stability and significantly decreased PLP specificity (Fig. 4*A*-*C* and *SI Appendix*, Figs. S3 and S6), suggesting that the C-terminal domain may have evolved to mediate high-affinity recruitment of PLP, a key step for efficient enzymatic degradation

of L-Met. These data also underscore the functional importance of the loop architecture. Given their apparent adaptability, these loops represent promising targets for protein engineering. Loop engineering has been demonstrated to extend the functional landscape of enzymes by modulating their activity, specificity and selectivity and may enable the rational design of enzymes with enhanced cofactor-binding capabilities at the distal part of the enzyme.(26-28)

Above all, these observations support the hypothesis that MGLs evolved a PLP-trapping mechanism in which a conserved Ser facilitates selective PLP recruitment at a structural motif near the entrance to the active site. The identification of this conserved, specific interaction between Ser located at the C-terminal domain and PLP in MGLs advances our understanding of PLP recognition and recruitment by enzymes, offering mechanistic insights into the molecular evolution of PLP-dependent enzymes. Furthermore, this knowledge provides a rational framework for the engineering and design of enzymes with enhanced or altered cofactor specificity.

## METHOD

### Crystallization and structure determination of yMGL

yMGL was expressed in *E. coli* and purified by nickel affinity chromatography following the method described by Zhao *et al.*(16) and then yMGL was further purified by an anion charge column Resource Q (GE Lifesciences) and Superdex200 Increase 10/300GL gel-filtration column (GE Healthcare) following the method described by Jia.(29) yMGL was incubated with 0.2 mM PLP and 1 mM L-Met for 30 min before being subjected to crystallization screening at 4 °C. The crystallization condition for the best diffracted crystal was 0.2 mol/L NaCl, 0.1 mol/L CAPS, pH 10.3, 20% PEG8000, and 11 mg/mL yMGL. Diffraction data were collected on beamline BL02U1 at the Shanghai Synchrotron Radiation Facility (SSRF). X-ray diffraction data were collected from a single crystal at 100 K using

a monochromatic X-ray at a wavelength of 0.97918 Å. The data were processed and scaled by XDS (PMID: 20124692) and Aimless (PMID: 27275144). The structure of yMGL in complex with L-Met was solved by molecular replacement with the program Phaser (PMID: 19461840) using the model built by AlphaFold as the template. Several rounds of manual building by Coot (PMID: 15572765) and refinement by Phenix (PMID: 20124702) were carried out. The statistics of X-ray data collection and refinement are summarized in *SI Appendix*, Table S1. Structure figures were prepared by PyMOL (The PyMOL Molecular Graphics System, Version 1.2r3pre, Schrödinger, LLC.).

**Mutagenesis of MGLs**

The pET28a plasmid was used to express MGLs and their mutants. A Mut Express® II Fast Mutagenesis Kit V2 (Vazyme, Nanjing, Jiangsu Province, China) was used to mutate amino acid residues by using the primers detailed in *SI Appendix*, Table S2. The PCR amplification products were digested by *Dpn*I to remove the template DNA and then used directly in the recombination reaction. pET28a containing the genes encoding MGLs and their mutants was subsequently transformed into *E. coli* BL21 (DE3). Single colonies with the target mutation were inoculated into LB culture media supplemented with 50 μg/mL kanamycin and cultured overnight at 37 °C. After the optical density at 600 nm approached 0.8, 0.5 mM isopropyl thiogalactoside (IPTG) was added to the medium to induce the expression of MGLs and their mutants at 18 °C. After growing for 20 h, the cells were harvested by centrifugation, after which the MGLs and their mutants were purified.

**MGL activity determination**

The purified MGLs were treated with phenylhydrazine hydrochloride to remove the naturally bound PLP following the protocol.(30, 31) MGL activity was assayed following the method described by Zhao *et al.*(16) The concentration of L-Met (Shanghai Aladdin Biochemical Technology Co., Ltd., 99% pure) was 20 mM, and the concentration of PLP (TCI (Shanghai) Development Co., Ltd., over

98% pure) was 5 mM in a total volume of 1 mL of reaction mixture with 0.6 mg of the purified MGLs added. The inactivated enzymes (after boiling for 10 min) were used as the control. HPLC (Dionex UltiMate 3000, Thermo) with a Reprosil-Pur Basic C18 column (4.6 mm × 250 mm × 5 μm) from Dr Maisch GmbH (Germany) was used to analyze the decrease in the L-Met concentration and the production of α-ketobutyrate. A 13%/87% acetonitrile/water mixture adjusted to pH 3.0 with $H_3PO_4$ was used as the mobile phase, and the detection wavelength was 230 nm. The kinetic stability ($t_{1/2}$) and thermodynamic stability ($T_m$) of yMGL and its mutant were measured following methods of Hu *et al.*(19)

**Determination of the kinetics, CD and binding affinity**

The enzymatic degradation of L-Met was assessed in a final 1 mL volume containing various concentrations (0.1--50 mM) of L-Met, 5 μM PLP, 50 mM Tris-HCl buffer (pH 8.0) containing 3% NaCl and 0.6 mg/mL yMGL and its mutants. The reactions were performed at 20 °C for 10 min, after which 5 μL of $H_3PO_4$ (10 M) was added to the mixture to quench the reactions. To determine the kinetics of PLP, the PLP concentration was varied from 0.1 to 20 μM, and the L-Met concentration was fixed at 20 mM. The production of α-ketobutyric acid from L-Met was detected by reaction with MBTH following a method described previously.(32) The kinetics of hMGL were determined following the method described by Hu *et al.*(19)

A Chirascan V100 Spectrometer (Applied Photophysics, Leatherhead, Surrey, UK) was used to measure the CD spectra of yMGL and its truncation mutant. Both were suspended in 50 mM $Na_2HPO_4/NaH_2PO_4$ (pH 8.0) buffer at equal molar concentrations, and then CD spectra were obtained from 190 to 280 nm (a step size of 1 nm, 0.5 s time-per-point, 1 nm bandwidth). After the baseline was corrected, each sample was scanned three times to obtain the spectrum.

The interaction between PLP and yMGL or its mutants was analyzed using a Nicoya

OpenSPRTM system at 20 °C following the method described by Tan *et al.*(33) yMGL or its mutants were immobilized on the sensor Chip NTA (Cat. No. SEN-AU-100-10-NTA). PLP was injected as an analyte at various concentrations, and PBS (pH 8.0) was used as the running buffer to determine the $K_a$ (association rate), $K_d$ (dissociation rate), and KD (equilibrium dissociation constant that reflects the affinity for substrates).

**Deletion or truncation of yMGL in *Y. lipolytica***

The optimal gRNA sequence (20 bp) targeting yMGL was selected by using CHOPCHOP (https://chopchop.cbu.uib.no/), with W29 as the genetic background.(34). The plasmid pCfB3405 was used in this study to construct vectors harboring a single gRNA expression cassette.(35) The genomic DNA of W29 was used as a template for amplifying endogenous fragments that overlapped to generate seamlessly integrated fragments. To obtain a recombinant strain, the integrated fragments and specific gRNA plasmids were mixed and transformed into *Y. lipolytica* by using the lithium acetate-mediated yeast transformation method.(35)

α-Ketobutyric acid is the main product of L-Met degradation. 3-Methyl-2-benzothiazolone hydrazone hydrochloride (MBTH) was used to detect the extracellular and intracellular accumulation of keto acid following the method described by Stone *et al.*(32) The fermentation broth was sampled dynamically and then centrifuged at 12,000 × g for 10 min. The supernatant was filtered and then reacted with MBTH to detect the extracellular accumulation of keto acid. The cell pellets were washed and resuspended in 1 mL of 1% (v/v) formic acid, after which the mixture was incubated for 10 min at 95 °C to react with MBTH and detect the intracellular accumulation of keto acid.

*Y. lipolytica* was cultured in minimal medium. Its RNA was extracted using the E.Z.N.A. A yeast RNA kit (Omega Bio-Tek, Norcross, USA) was used, and total RNA was quantified using an Agilent 2100 Bioanalyzer (Agilent, CA, USA). RNA integrity was determined using an Agilent Bioanalyzer

4150 system (Agilent Technologies). RNA-seq libraries were prepared using the BGI Optimal mRNA-seq Lib Prep Kit (BGI-Shenzhen, China). PE100/PE150 sequencing was performed on a G400/T7/T10 sequencer (BGI-Shenzhen, China) using combined probe anchor polymerization (cPAS) technology. Clean reads were separately aligned to the reference genome in orientation mode using HISAT2 software (http://daehwankimlab.github.io/hisat2/) to obtain mapped reads. Differential expression analysis was performed via DESeq2, and DEGs with $|\log2FC| > 1$ and adjusted $P < 0.05$ were considered significantly DEGs.

*Y. lipolytica* cells and fermentation supernatant samples were analyzed via a Vanquish ultrahigh-performance liquid chromatography (UHPLC) system (Mercedes-Benz, Bremen, Germany) on day 3. After the raw LC–MS data were calibrated, the MS information was simultaneously matched with the metabolism public database HMDB and the Majorbio cloud platform (https://www.majorbio.com/) to obtain the metabolite information of α-ketobutyric acid.

**Molecular modeling and phylogenetic analysis of MGLs**

A nonrooted molecular phylogenetic tree of the MGLs from *Homo sapiens*, *Trichomonas vaginalis*, *Entamoeba histolytica*, *Saccharomyces cerevisiae*, *Kluyveromyces lactis* and *Yarrowia lipolytica*, which are eukaryotes; *Pseudomonas putida*; *Citrobacter freundii*; *Clostridium sporogenes*; and *Micromonospora echinospora*, which are prokaryotes, was established through ClustalW multiple sequence alignment via the maximum likelihood method in MEGA X 10.0.4. The phylogenetic relationships of MGLs from yeast were analyzed via the fast minimum evolution method at the website (https://blast.ncbi.nlm.nih.gov/Blast.cgi). MGLs and their mutants in enzymatic reactions were modeled via AlphaFold3 structural prediction via a web server (https://alphafoldserver.com/)(36) and visualized in ChimeraX. The entrance of yMGL was predicted via CAVER software (https://loschmidt.chemi.muni.cz/hotspotwizard/) and displayed.(37) AutoDock software was used to

analyze the interaction between PLP and MGLs. The ancestral sequence of yMGL was reconstructed through the FireProt-ASR online service at the website (http://loschmidt.chemi.muni.cz/fireprotasr/).(38)

## SUPPORTING INFORMATION

Cold tolerance of yMGL, Enzymatic characterization of yMGL and yMGL-ΔCTD, Kinetic constants for yMGL (**A, B**) and yMGL-ΔCTD (**C, D**), Verification of the deletion of yMGL and the sequence encoding its C-terminal region, Thermal shift assay results for yMGL and its mutant yMGL-S333A, Simulation of the interaction between PLP and yMGL-ΔCTD, Data and refinement statistics for the structures of yMGL and primers used for constructing the yMGL mutants.

## ACKNOWLEDGEMENTS

This work was supported by the National Key Research and Development Program of China (2022YFC2106100), the National Natural Science Foundation of China (Grant Nos. 31570054, 22377098 and 21807088), the Key Project of Hubei Provincial Department of Education (T2022011) and the State Key Laboratory of Microbial Technology Open Projects Fund (Project No. M2022-06). We thank the SSRF BL02U1 beam line for data collection and processing.

## AUTHOR CONTRIBUTIONS

Conceptualization: K.Z.J., X.C., L.W.Z. and J.F.H. Formal analysis: K.Z.J., X.C., C.Y., X.T.L. and M.W.S. Funding acquisition: K.Z.J., X.C. and L.W.Z. Investigation: C.Y., X.T.L., M.W.S., Z.G., Y.C. and R.Q.S. Methodology: C.Y., X.T.L. and M.W.S. Project administration: K.Z.J., X.C. and L.W.Z. Resources: C.Y., X.T.L., M.W.S., Z.G., and Y.C. Supervision: K.Z.J., X.C. and Z.J.D. Validation: C.Y., X.T.L., M.W.S., Z.G., Y.C. Writing – original draft: K.Z.J., X.C., C.Y. and X.T.L. Writing – review

& editing: K.Z.J., X.C. and C.Y.

## RERERENCES


1. Hoffarth ER, *et al.* A shared mechanistic pathway for pyridoxal phosphate-dependent arginine oxidases. *Proc. Natl. Acad. Sci. U.S.A.* **118**, e2012591118 (2021).
2. Wilson MP, Plecko B, Mills PB, & Clayton PT, Disorders affecting vitamin B(6) metabolism. *J. Inherit. Metab. Dis.* **42**, 629-646 (2019).
3. Ling LL, *et al.* A new antibiotic kills pathogens without detectable resistance. *Nature* **517**, 455-459 (2015).
4. Hoffarth ER, Rothchild KW, & Ryan KS, Emergence of oxygen- and pyridoxal phosphate-dependent reactions. *Febs. J.* **287**, 1403-1428 (2020).
5. Hoegl A, *et al.* Mining the cellular inventory of pyridoxal phosphate-dependent enzymes with functionalized cofactor mimics. *Nat. Chem.* **10**, 1234-1245 (2018).
6. Daniel-Ivad P & Ryan KS, New reactions by pyridoxal phosphate-dependent enzymes. *Curr. Opin. Chem. Biol.* **81**, 102472 (2024).
7. Li Z, Zhao Y, Zhou H, Luo HB, & Zhan CG, Catalytic roles of coenzyme pyridoxal-5'-phosphate (plp) in plp-dependent enzymes: reaction pathway for methionine-gamma-lyase-catalyzed l-methionine depletion. *ACS Catal.* **10**, 2198-2210 (2020).
8. Du YL & Ryan KS, Pyridoxal phosphate-dependent reactions in the biosynthesis of natural products. *Nat. Prod. Rep.* **36**, 430-457 (2019).
9. Kirschning A, Coenzymes and their role in the evolution of life. *Angew. Chem. Int. Ed. Engl.* **60**, 6242-6269 (2021).
10. Maeda HA & Fernie AR, Evolutionary history of plant metabolism. *Annul. Rev. of Plant Biol.* **72**, 185-216 (2021).
11. Cunchillos C & Lecointre G, Evolution of amino acid metabolism inferred through cladistic

analysis. *J. Biol. Chem.* **278**, 47960-47970 (2003).

12. Koper K, Han S-W, Pastor DC, Yoshikuni Y, & Maeda HA, Evolutionary origin and functional diversification of aminotransferases. *J. Biol. Chem.* **298**, 102122 (2022).
13. Goldman AD & Kacar B, Cofactors are remnants of life's origin and early evolution. *J. Mol. Evol.* **89**, 127-133 (2021).
14. Zabinski RF & Toney, MDMetal ion inhibition of nonenzymatic pyridoxal phosphate catalyzed decarboxylation and transamination. *J. Am. Chem. Soc.* **123**, 193-198 (2001).
15. Kolluru GK, Shackelford RE, Shen X, Dominic P, & Kevil CG, Sulfide regulation of cardiovascular function in health and disease. *Nat. Rev. Cardiol.* **20**, 109-125 (2023).
16. Zhao QL, Wang ZL, Yang L, Zhang S, & Jia KZ, YALI0C22088g from *Yarrowia lipolytica* catalyses the conversion of l-methionine into volatile organic sulfur-containing compounds. *Microb. Biotechnol.* **14**, 1462-1471 (2021).
17. Green CL, Lamming DW, & Fontana L. Molecular mechanisms of dietary restriction promoting health and longevity. *Nat. Rev. Mol. Cell. Bio.* **23**, 56-73 (2022).
18. Lu WC, *et al.* Enzyme-mediated depletion of serum l-Met abrogates prostate cancer growth via multiple mechanisms without evidence of systemic toxicity. *Proc. Natl. Acad. Sci. U.S.A.* **117**, 13000-13011 (2020).
19. Hu Y, *et al.* Depletion of l-methionine in foods with an engineered thermophilic methionine gamma-lyase efficiently inhibits tumor growth. *J. Agric. Food. Chem.***71**, 17141–17152. (2023).
20. Feller G & Gerday C, Psychrophilic enzymes: hot topics in cold adaptation. *Nat. Rev. Microbiol.* **1**, 200-208 (2003).
21. Su D, Kosciuk T, Yang M, Price IR, & Lin H (2021) Binding Affinity Determines Substrate Specificity and Enables Discovery of Substrates for N-Myristoyltransferases. *Acs Catal.* 11,

14877-14883.

22. Yang W, *et al.* Mitochondrial sirtuin network reveals dynamic sirt3-dependent deacetylation in response to membrane depolarization. *Cell* **167,** 985-1000.e1021 (2016).

23. Someya S, *et al.* Sirt3 mediates reduction of oxidative damage and prevention of age-related hearing loss under caloric restriction. *Cell* **143**, 802-812 (2010).

24. Hébert A, *et al.* New insights into sulfur metabolism in yeasts as revealed by studies of *Yarrowia lipolytica*. *Appl. Environ. Microb.* **79**,1200-1211 (2013).

25. Corbella M, Pinto GP, & Kamerlin SCL, Loop dynamics and the evolution of enzyme activity. *Nat. Rev. Chem.* **7**, 536-547(2023).

26. Gu J, Xu Y, & Nie Y, Role of distal sites in enzyme engineering. *Biotechnol. Adv.* **63**, 108094 (2023).

27. Campbell EC, *et al.* Laboratory evolution of protein conformational dynamics. *Curr. Opin. Struct. Biol.* **50**, 49-57 (2018).

28. Pinto GP, Corbella M, Demkiv AO, & Kamerlin SCL, Exploiting enzyme evolution for computational protein design. *Trends. Biochem. Sci.* **47**, 375-389(2022).

29. Jia KZ, *et al.* Demethiolase STR3 controls the conversion of methionine into methanethiol. *Sci. Rep.* **6**, 21920. (2016).

30. Allegrini A, Astegno A, La Verde V, & Dominici P, Characterization of C-S lyase from *Lactobacillus delbrueckii subsp. bulgaricus* ATCC BAA-365 and its potential role in food flavour applications. *J. Biochem.* **161**, 349-360. (2016).

31. Bertoldi M, Cellini B, Clausen T, & Voltattorni CB, Spectroscopic and kinetic analyses reveal the pyridoxal 5'-phosphate binding mode and the catalytic features of *Treponema denticola* cystalysin. *Biochemistry* **41**, 9153-9164 (2002).

32. Stone E, *et al. De Novo* Engineering of a human cystathionine-γ-lyase for systemic L-methionine depletion cancer therapy. *ACS Chem. Biol.* **7**, 1822-1829 (2012).

33. Tan FF, *et al.* Engineering the entrance of a flavonoid glycosyltransferase promotes the glycosylation of etoposide aglycone. *ACS Synth. Biol.* **11**,1874-1880 (2022).

34. Labun K, *et al.* CHOPCHOP v3: expanding the CRISPR web toolbox beyond genome editing. *Nucleic. Acids Research* **47**, W171-W174 (2019).

35. Holkenbrink C, *et al.* EasyCloneYALI: CRISPR/Cas9-based synthetic toolbox for engineering of the Yeast *Yarrowia lipolytica*. *Biotechnol. J.* **13**, e1700543. (2018).

36. Abramson J, *et al.* Accurate structure prediction of biomolecular interactions with AlphaFold 3. *Nature* **630**, 493-500 (2024).

37. Pettersen EF, *et al.* UCSF ChimeraX: Structure visualization for researchers, educators, and developers. *Protein Sci.* **30**, 70-82 (2020).

38. Musil M, *et al.* FireProtASR: A web server for fully automated ancestral sequence reconstruction. *Brief. Bioinform.* **22**, bbaa337 (2021).

# FIGURE LEGENDS

**Fig. 1. Phylogenetic and structural features of yMGL.** (**A**) Phylogenetic relationships of MGLs from eukaryotes (*Homo sapiens*, *Trichomonas vaginalis*, *Entamoeba histolytica*, *Saccharomyces cerevisiae*, *Kluyveromyces lactis*, and *Yarrowia lipolytica*) and prokaryotes (*Pseudomonas putida*, *Citrobacter freundii*, *Clostridium sporogenes*, and *Micromonospora echinospora*). yMGL, representing the newly identified cystathionine γ-lyase group, is shaded in cyan, and the other MGLs belonging to the cystathionine γ-lyase family are shaded in green. Cystathionine β-lyases from yeast are shaded in ochre. (**B**) Crystal structure of yMGL. The active sites exist at the interface of the two monomers. The PLP binding domains, including residues 64-261, are marked with deeper colors. (**C**) A Schiff base was formed by PLP and K204 at the active site of chain A. L-Met was surrounded by the residues T332, R344 and R357. (**D**) Section of the simulated-annealing $2F_O$-$F_C$ composite omit map (black mesh) contoured at the 0.7σ level at the active site of chain A. (**E**) A Schiff base was formed by the catalytic residues K204 and PLP at the active site of chain B. L-Met was surrounded by the residues Y61, Y113, R344 and R357. (**F**) Section of the simulated-annealing $2F_O$-$F_C$ composite omit map (black mesh) contoured at the 1.0 σ level at the active site of chain B. The electron density for PLP in chain B is better resolved than that in chain A, likely because the absence of loop 53-64 is inferred to be involved in the interaction with PLP in chain B and its presence in chain A.

**Fig. 2. Key residues in yMGL.** (**A**) Identification of key amino acid residues in yMGL. The amino acid residues in the entrance and active sites were mutated to Ala, and their activity was subsequently determined to identify the key amino acid residues. Only one key amino acid residue (S333) is located in the C-terminal region, which is shown with a deeper color. (**B**) Overview of the entrance and active sites of yMGL. (**C, D**) The key amino acid residues constituting the entrance (**C**) and active sites (**D**)

are marked in color corresponding to the monomers of yMGL. The key amino acid residues are shown in stick style. (**E**) Aligning the amino acid sequence of yMGL with pMGL (PDB ID: 2O7C) and hMGL with higher L-Met lysis activity. Identical amino acid residues are in black, and similar amino acid residues are in gray. Dashes represent gaps for improving the alignment. Secondary structure information was obtained from yMGL and presented as a ribbon diagram (H: Helix; S: Sheet). The truncated C-terminal domain is shaded, and the cleavage site is located in the conserved amino acid segment outside the C-terminal domain and marked with a triangular wedge.

**Fig. 3. C-terminal truncation increases the molecular weight and increases the L-Met lysis activity of multimers.** (**A**) Truncation of the C-terminal region of yMGL. (**B, C**) SDS–PAGE analysis of yMGL and its truncation mutant yMGL-ΔCTD. The theoretical monomer molecular weights of yMGL are 41.93 (**B**) and 27.77 (**C**) kDa, which is consistent with the SDS–PAGE results. (**D**) Purification of yMGL and yMGL-ΔCTD by size exclusion chromatography. yMGL and yMGL-ΔCTD exist as polymers in the enzymatic reaction solution, while the molecular weight of yMGL-ΔCTD is greater than that of yMGL. (**E**) Dynamic light scattering analysis of yMGL and yMGL-ΔCTD. The size of yMGL-ΔCTD is larger than that of yMGL. (**F**) yMGL-ΔCTD exhibited higher L-Met lysis activity than yMGL did. The activity of yMGL at 20 °C was 299.06 ± 1.77 nmol·min$^{-1}$· mg recombinant protein$^{-1}$ and was set at 1.0.

**Fig. 4. The C-terminal region specifically interacts with PLP and determines L-Met degradation in *Y. lipolytica*.** (**A**) yMGL shows strong binding affinity for PLP. $K_a$=8.07 × 10$^{1}$ M$^{-1}$·s$^{-1}$, $K_d$=2.67 × 10$^{-3}$ s$^{-1}$, KD=3.31 × 10$^{-5}$ M. (**B**) No binding affinity between PLP and yMGL-ΔCTD. (**C**) Binding affinity between PLP and yMGL-CTD (C-terminal domain) approaches yMGL. $K_a$=1.74 × 10$^{2}$ M$^{-1}$·s$^{-}$

$^{1}$, $K_d$=1.79 × $10^{-3}$ $s^{-1}$, KD=1.03 × $10^{-5}$ M. (**D**) Deletion of *yMGL* and the sequence encoding the C-terminal domain obviously increase the cell density. The addition of L-Met had no obvious effect on cell growth. $OD_{600}$, absorbance at 600 nm. (**E, F**) Deletion of the sequence encoding the C-terminal domain and *yMGL* markedly decreased the accumulation of intracellular (**E**) and extracellular (**F**) keto acids, respectively. (**G**) Deletion of the sequence encoding the C-terminal domain significantly diminished the expression of *yMGL* at the transcriptional level. (**H, I**) The accumulation of α-ketobutyrate. Deletion of the sequence encoding the C-terminal domain resulted in reduced intracellular (**H**) and extracellular (**I**) accumulation of α-ketobutyrate. The addition of L-Met markedly increased α-ketobutyrate accumulation in the wild-type strain.

**Fig. 5. Identification of key amino acid residues that specifically interact with PLP**. (**A**) Screening the amino acid residues with the potential to specifically interact with PLP. R255, K270 and S333 were inferred to interact with PLP and exhibited a ball style. S333 is adjacent to the entrance or located at the active site. (**B, C**) S333 has no direct interaction with PLP at the active site. At the active site of chain A (**B**), PLP forms a Schiff base with K204 and has no direct interaction with S333. At the active site of chain B (**C**), S333 anchored near L-Met and had no direct interaction with PLP. (**D**) Mutating S333 into Ala in yMGL sharply decreases its specificity for PLP. $K_a$=2.08 × $10^{1}$ $M^{-1}\cdot s^{-1}$, $K_d$=1.96 × $10^{-2}$ $s^{-1}$, KD=9.42 × $10^{-4}$ M (yMGL-S333A). Compared with yMGL, the binding affinity of the yMGL-S333A mutant for PLP decreased by 27.54-fold. (**E, F**) The binding affinity toward PLP was characterized via a thermal shift assay. The addition of PLP increased the enzymatic melting temperature ($T_m$), whereas the S333A mutation obviously reduced the $T_m$ compared with that of yMGL, indicating that its specificity for PLP decreased. (**G**) Time evolution of the root-mean-square deviations of yMGL and yMGL-S333A. (**H**) Root mean square fluctuations of yMGL and yMGL-

S333A. S333 is located at the loop, while the mutation did not trigger obvious fluctuations in the whole yMGL structure.

**Fig. 6. Functional identification of S340 in hMGL.** (**A**) S340 situated at the proximity of the entrance of the hMGL. The entrance and active sites are predicted to occur at the interface of the dimer; K212 is the inferred catalytic residue and is shown as a red ball-and-stick model. S340 in hMGL is conserved with S333 in yMGL and is shown as a blue ball model. The C-terminal regions in each monomer are marked with deeper colors. (**B, C**) The binding affinity toward PLP was characterized via a thermal shift assay. The addition of PLP increased the enzymatic melting temperature ($T_m$), whereas the S340A mutation obviously reduced the $T_m$ compared with that of hMGL, indicating that its specificity for PLP decreased.

**Fig. 7. Ancestral reconstruction of yMGL reveals the conservation of Ser.** (**A**) Ser is conserved in yMGL and its ancestor enzymes. A phylogenetic tree was constructed by using the NCBI database and the FireProt website to infer the ancestor enzymes of yMGL, and the ancestor enzymes included ASR195, ASR194, ASR193, ASR192, ASR190, ASR189, ASR188, ASR187, ASR186 and ASR151. Cystathionine γ-synthases, cystathionine γ-lyases, aminotransferases, cystathionine β-lyases, hypothetical proteins and MGLs dependent on PLP with accession numbers were provided by the FireProt website to search for ancestor enzymes and are shown in blue, red, purple, brown, black and green, respectively. (**B**) yMGL functions as a cystathionine γ-synthase. Succinic acid was produced in the enzymatic system p]using L-cysteine and O-succinyl-L-homoserine as the substrates and was identified via MS/MS. L-Cystathionine was not detected because yMGL possesses L-cystathionine degradation capacity.(16) (**C**) yMGL is clustered with the cystathionine γ-lyase 4U2H and the

cystathionine γ-synthases 6LD7 and 1CS1, forming a distinct phylogenetic tree branch. yMGL may have retained the promisuity characteristic of its ancestors. (**D**) Structural superposition of the enzymes marked with asterisks in Fig. 7*C* (yMGL, 1N8P, 1I41, 1CS1, 4U2H, 3JW9, ASR151, ASR195). The Ser residue (marked with a red arrow) is conserved and located on a trap-like structure near the enzyme's entrance. The ASR151 and ASR195 models were constructed by using AlphaFold 3. (**E**) Multiple sequence alignment of the eight proteins. The Ser residue (marked with a red arrow) is strictly conserved in enzymes, including yMGL, 1N8P, 1I41, 1CS1, 4U2H, 3JW9, ASR151 and ASR195.

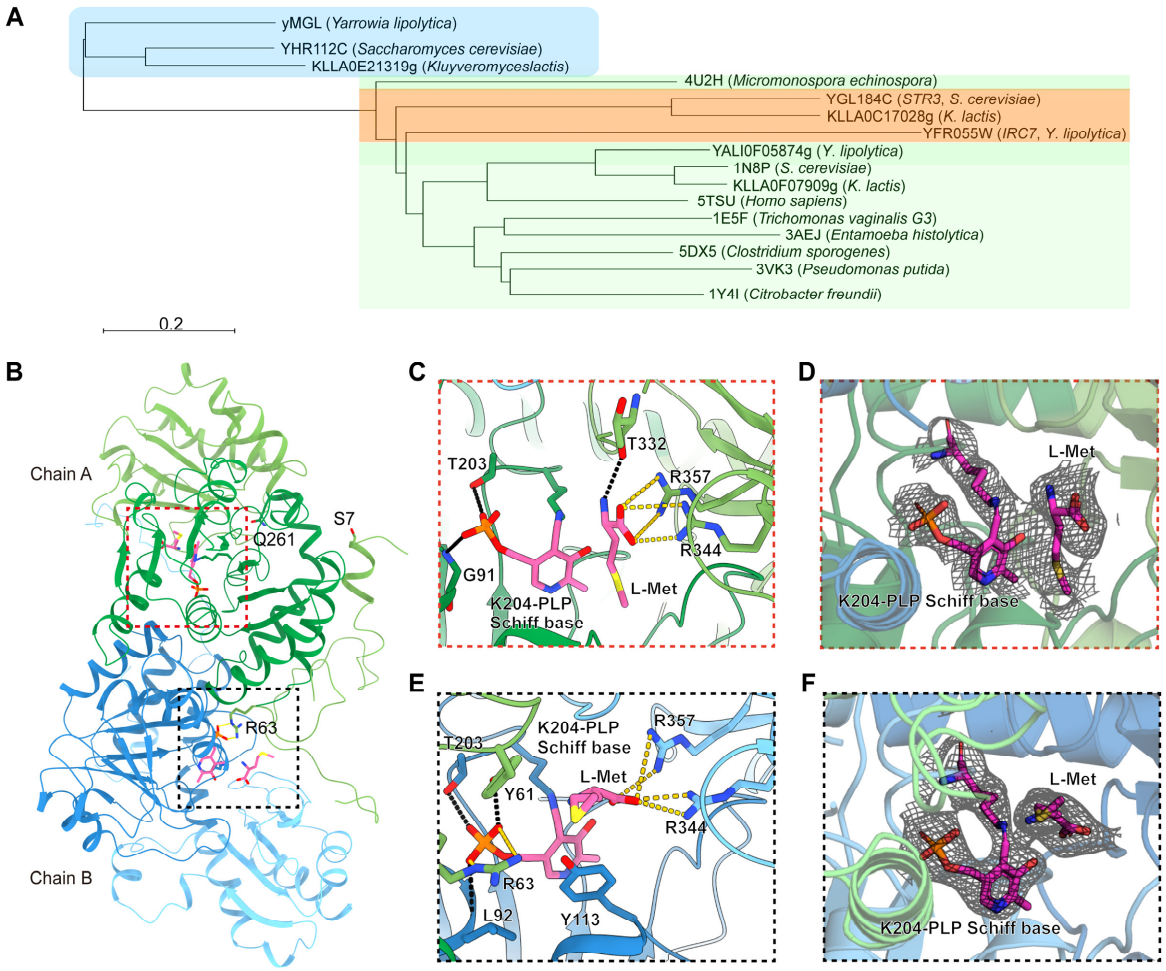
A
yMGL (Yarrowia lipolytica)
YHR112C (Saccharomyces cerevisiae)
KLLA0E21319g (Kluyveromyceslactis)
4U2H (Micromonospora echinospora)
YGL184C (STR3, S. cerevisiae)
KLLA0C17028g (K. lactis)
YFR055W (IRC7, Y. lipolytica)
YALI0F05874g (Y. lipolytica)
1N8P (S. cerevisiae)
KLLA0F07909g (K. lactis)
5TSU (Homo sapiens)
1E5F (Trichomonas vaginalis G3)
3AEJ (Entamoeba histolytica)
5DX5 (Clostridium sporogenes)
3VK3 (Pseudomonas putida)
1Y4I (Citrobacter freundii)
0.2
B
Chain A
S7
Q261
R63
Chain B
C
T332
T203
R357
R344
G91
L-Met
K204-PLP
Schiff base
D
L-Met
K204-PLP Schiff base
E
K204-PLP
Schiff base
R357
T203
L-Met
Y61
R344
R63
L92
Y113
F
L-Met
K204-PLP Schiff base

**Fig. 1.**

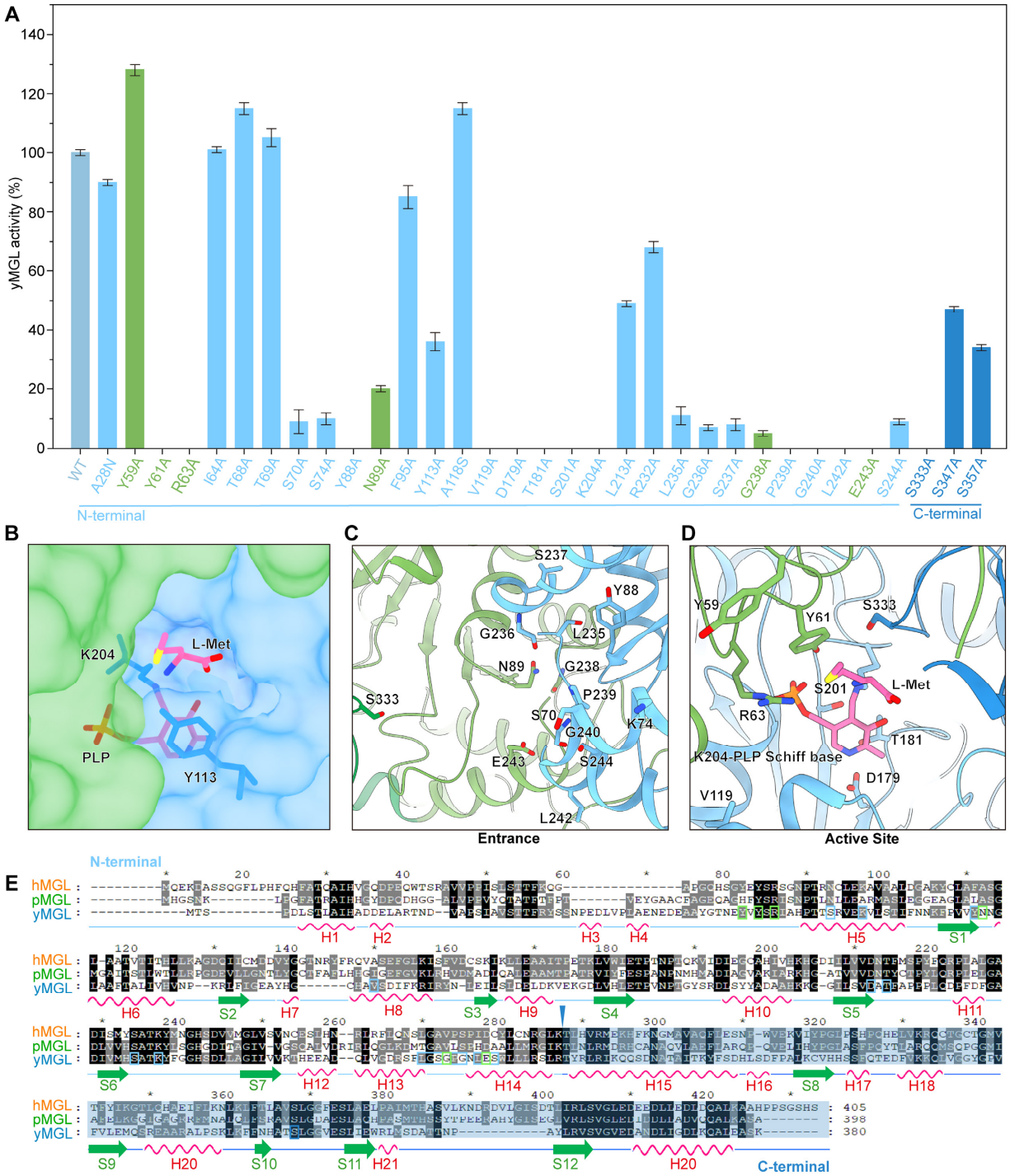
A
yMGL activity (%)
0
20
40
60
80
100
120
140
WT
A28N
Y59A
Y61A
R63A
I64A
T68A
T69A
S70A
S74A
Y88A
N89A
F95A
Y113A
A118S
V119A
D179A
T181A
S201A
K204A
L213A
R232A
L235A
G236A
S237A
G238A
P239A
G240A
L242A
E243A
S244A
S333A
S347A
S357A
N-terminal
C-terminal
B
K204
L-Met
PLP
Y113
C
S237
Y88
G236
L235
N89
G238
S333
P239
S70
K74
G240
E243
S244
L242
Entrance
D
Y59
Y61
S333
S201
L-Met
R63
T181
K204-PLP Schiff base
D179
V119
Active Site
E
N-terminal
hMGL :
pMGL :
yMGL :
H1
H2
H3
H4
H5
S1
H6
S2
H7
H8
S3
H9
S4
H10
S5
H11
S6
S7
H12
H13
H14
H15
H16
S8
H17
H18
S9
H20
S10
S11
H21
S12
H20
C-terminal

**Fig. 2.**

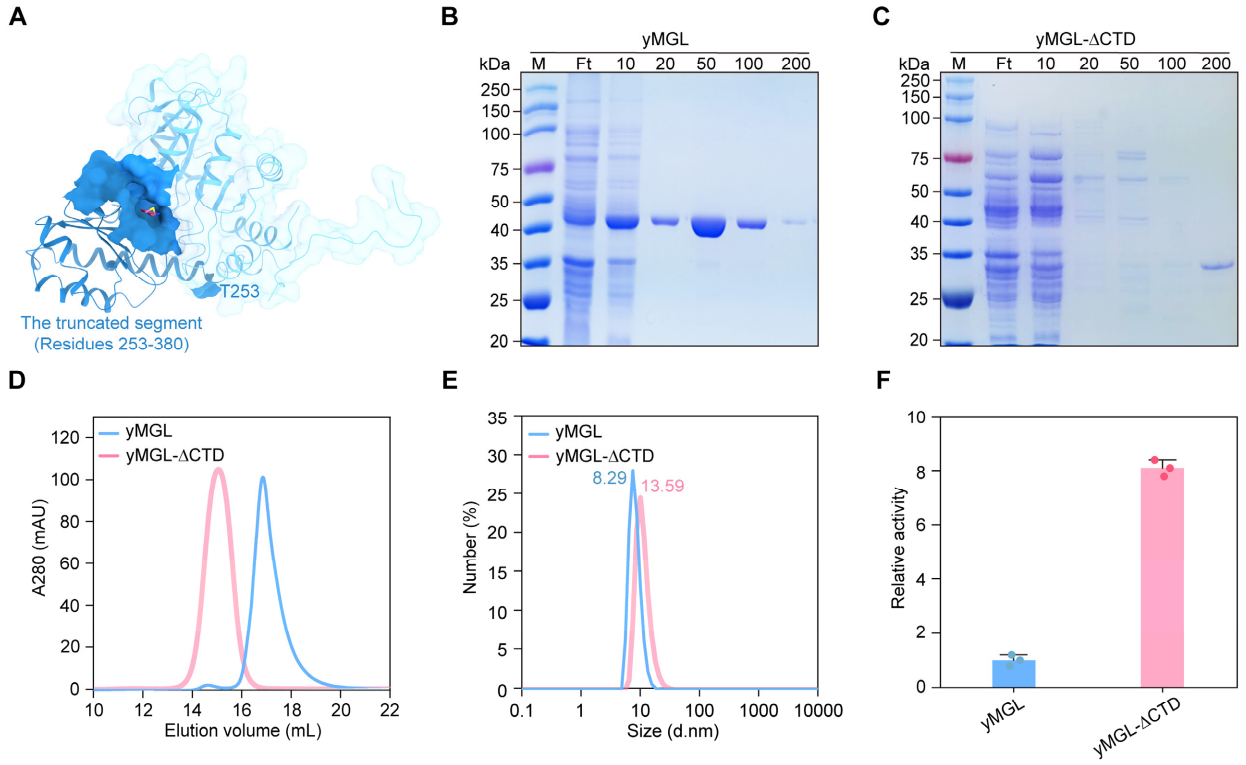
A
T253
The truncated segment
(Residues 253-380)
B
yMGL
kDa
M Ft 10 20 50 100 200
250
150
100
75
50
40
35
25
20
C
yMGL-ΔCTD
kDa
M Ft 10 20 50 100 200
250
150
100
75
50
40
35
25
20
D
yMGL
yMGL-ΔCTD
A280 (mAU)
Elution volume (mL)
E
yMGL
yMGL-ΔCTD
8.29
13.59
Number (%)
Size (d.nm)
F
Relative activity
yMGL
yMGL-ΔCTD

**Fig. 3.**

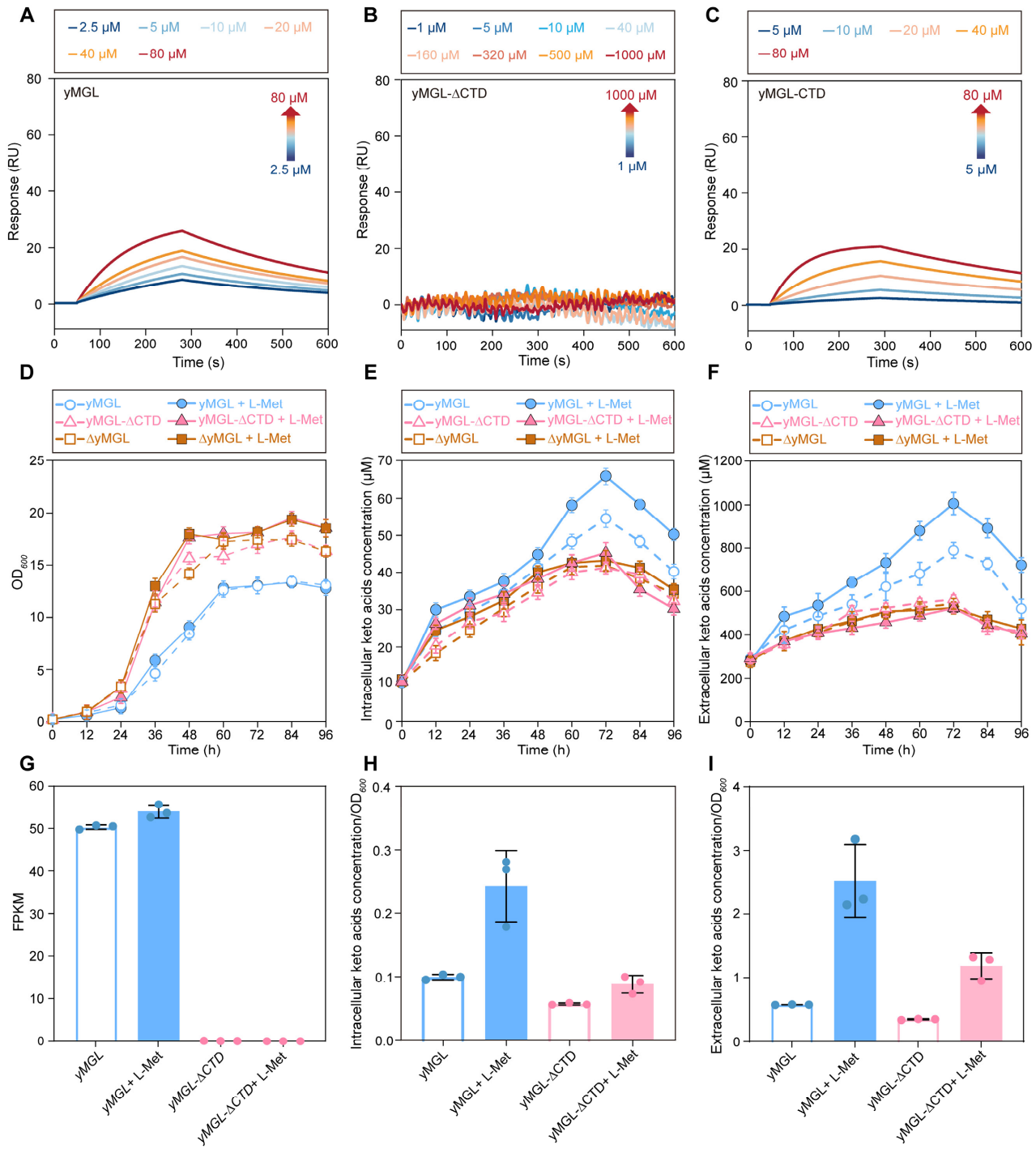
A
2.5 μM
5 μM
10 μM
20 μM
40 μM
80 μM
yMGL
80 μM
2.5 μM
Response (RU)
Time (s)
B
1 μM
5 μM
10 μM
40 μM
160 μM
320 μM
500 μM
1000 μM
yMGL-ΔCTD
1000 μM
1 μM
Response (RU)
Time (s)
C
5 μM
10 μM
20 μM
40 μM
80 μM
yMGL-CTD
80 μM
5 μM
Response (RU)
Time (s)
D
yMGL
yMGL + L-Met
yMGL-ΔCTD
yMGL-ΔCTD + L-Met
ΔyMGL
ΔyMGL + L-Met
OD600
Time (h)
E
Intracellular keto acids concentration (μM)
Time (h)
F
Extracellular keto acids concentration (μM)
Time (h)
G
FPKM
yMGL
yMGL+ L-Met
yMGL-ΔCTD
yMGL-ΔCTD+ L-Met
H
Intracellular keto acids concentration/OD600
I
Extracellular keto acids concentration/OD600

**Fig. 4.**

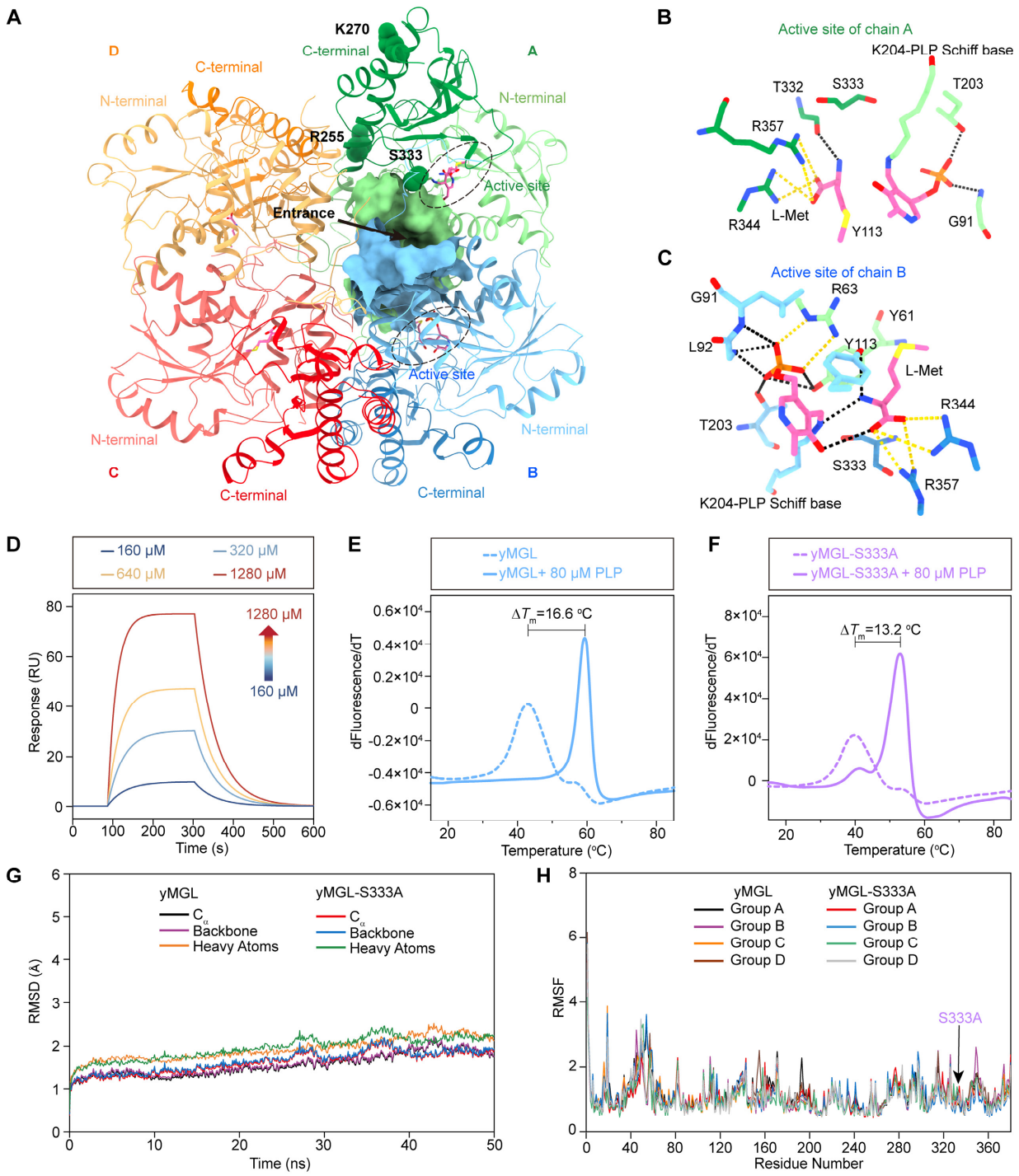
A
K270
C-terminal
D
A
C-terminal
N-terminal
N-terminal
R255
S333
Active site
Entrance
Active site
N-terminal
N-terminal
C
B
C-terminal
C-terminal
B
Active site of chain A
K204-PLP Schiff base
T332
S333
T203
R357
R344
L-Met
Y113
G91
C
Active site of chain B
G91
R63
Y61
L92
Y113
L-Met
R344
T203
S333
R357
K204-PLP Schiff base
D
160 μM
320 μM
640 μM
1280 μM
1280 μM
160 μM
Response (RU)
Time (s)
E
yMGL
yMGL+ 80 μM PLP
ΔTm=16.6 °C
dFluorescence/dT
Temperature (°C)
F
yMGL-S333A
yMGL-S333A + 80 μM PLP
ΔTm=13.2 °C
dFluorescence/dT
Temperature (°C)
G
yMGL
Cα
Backbone
Heavy Atoms
yMGL-S333A
Cα
Backbone
Heavy Atoms
RMSD (Å)
Time (ns)
H
yMGL
Group A
Group B
Group C
Group D
yMGL-S333A
Group A
Group B
Group C
Group D
S333A
RMSF
Residue Number

**Fig. 5.**

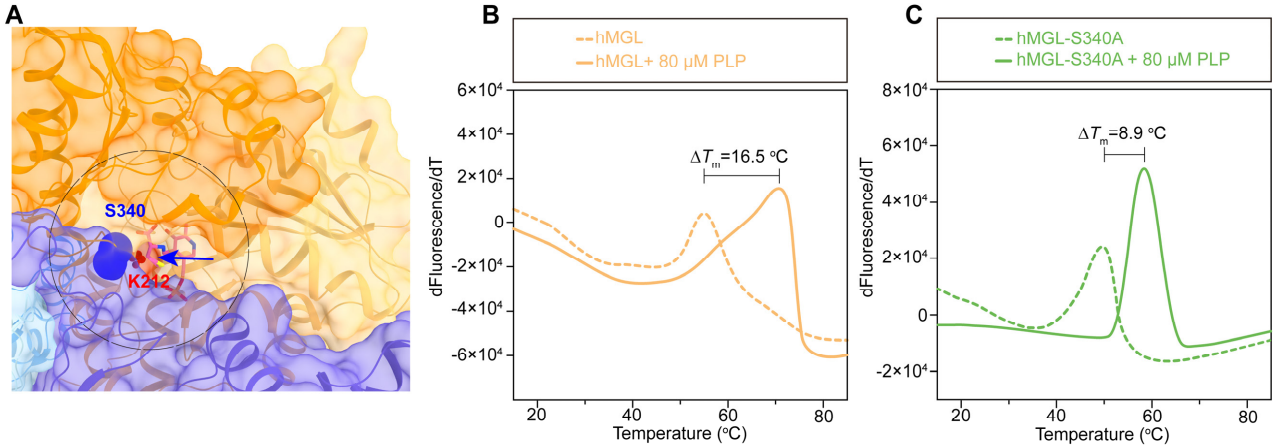
A
S340
K212
B
hMGL
hMGL+ 80 μM PLP
ΔTm=16.5 °C
dFluorescence/dT
Temperature (°C)
C
hMGL-S340A
hMGL-S340A + 80 μM PLP
ΔTm=8.9 °C
dFluorescence/dT
Temperature (°C)

**Fig. 6.**

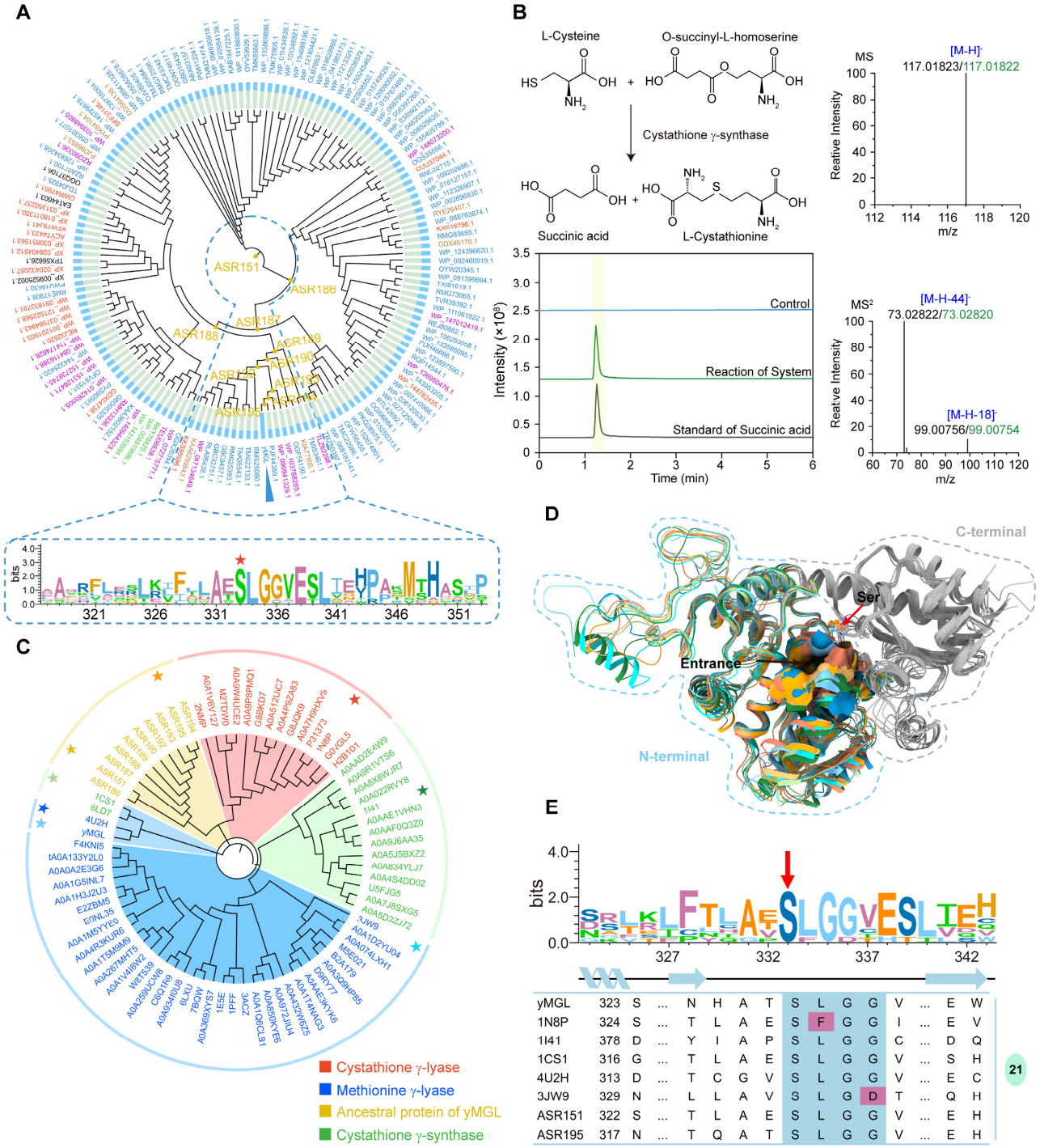
A
B
L-Cysteine
O-succinyl-L-homoserine
Cystathione γ-synthase
Succinic acid
L-Cystathionine
Control
Reaction of System
Standard of Succinic acid
Intensity (×10⁸)
Time (min)
MS
[M-H]⁻
117.01823/117.01822
Reative Intensity
m/z
MS²
[M-H-44]⁻
73.02822/73.02820
[M-H-18]⁻
99.00756/99.00754
C
D
C-terminal
Ser
Entrance
N-terminal
E
bits
Cystathione γ-lyase
Methionine γ-lyase
Ancestral protein of yMGL
Cystathione γ-synthase
yMGL 323 S ... N H A T S L G G V ... E W
1N8P 324 S ... T L A E S F G G I ... E V
1I41 378 D ... Y I A P S L G G C ... D Q
1CS1 316 G ... T L A E S L G G V ... S H
4U2H 313 D ... T C G V S L G G V ... E C
3JW9 329 N ... L L A V S L G D T ... Q H
ASR151 322 S ... T L A E S L G G V ... E H
ASR195 317 N ... T Q A T S L G G V ... E H
21

**Fig. 7.**

**Table 1. The parameters for kinetics and affinity.**

| yMGL and its mutants | L-Met and PLP | $K_m$ | $k_{cat}$ ($s^{-1}$) | $k_{cat}/K_m$ ($M^{-1}\cdot s^{-1}$) | $K_a$ ($M^{-1}\cdot s^{-1}$) | $K_d$ ($s^{-1}$) | KD (M) |
|---|---|---|---|---|---|---|---|
| yMGL | Saturated PLP, variable L-Met | 1.50 ± 0.01 mM | 0.06 ± 0.00 | 40.00 | | | |
| | Saturated L-Met, variable PLP | 0.85 ± 0.02 μM | 0.06 ± 0.00 | 70588.24 | $8.07 \times 10^{1}$ | $2.67 \times 10^{-3}$ | $3.31 \times 10^{-5}$ |
| yMGL-ΔCTD | Saturated PLP, variable L-Met | 0.75 ± 0.01 mM | 0.04 ± 0.00 | 53.33 | | | |
| | Saturated L-Met, variable PLP | 1.65 ± 0.00 μM | 0.01 ± 0.00 | 6060.61 | No PLP binding signals were detected | | |
| yMGL-CTD | Saturated PLP, variable L-Met | Had no activity with L-Met | | | | | |
| | Saturated L-Met, variable PLP | Had no activity with L-Met | | | $1.74 \times 10^{2}$ | $1.79 \times 10^{-3}$ | $1.03 \times 10^{-5}$ |